Check for updates

ADVANCED MATERIALS
www.advmat.de

Efficient Electron Transport Layer Free Small-Molecule Organic Solar Cells with Superior Device Stability

*Haijun Bin, Junke Wang, Junyu Li, Martijn M. Wienk, and René A. J. Janssen**

Electron transport layers (ETLs) placed between the electrodes and a photoactive layer can enhance the performance of organic solar cells but also impose limitations. Most ETLs are ultrathin films, and their deposition can disturb the morphology of the photoactive layers, complicate device fabrication, raise cost, and also affect device stability. To fully overcome such drawbacks, efficient organic solar cells that operate without an ETL are preferred. In this study, a new small-molecule electron donor (H31) based on a thiophene-substituted benzodithiophene core unit with trialkylsilyl side chains is designed and synthesized. Blending H31 with the electron acceptor Y6 gives solar cells with power conversion efficiencies exceeding 13% with and without 2,9-bis[3-(dimethyloxidoamino)propyl]anthra[2,1,9-*def*:6,5,10-*d′e′f′*]diisoquinoline-1,3,8,10(2H,9H)-tetrone (PDINO) as the ETL. The ETL-free cells deliver a superior shelf life compared to devices with an ETL. Small-molecule donor–acceptor blends thus provide interesting perspectives for achieving efficient, reproducible, and stable device architectures without electrode interlayers.

1. Introduction

Organic solar cells (OSCs) receive extensive attention as future photovoltaic technology featuring a combination of unique advantages such as lightweight, semitransparency, flexibility, conformity, low cost, and being solution-processable at low temperatures. With recent revolutionary advances in nonfullerene acceptor (NFA) materials, power conversion efficiencies (PCEs) of OSCs are imminent to 20%.[1–6] Nowadays, many researchers focus on developing small-molecule nonfullerene acceptors and matching donor polymers. Hence, polymer solar cells (PSCs), composed of a polymer donor and a small-molecule acceptor, represent the state of the art.[7–13] However, batch-to-batch variations in conjugated polymer synthesis in terms of purity and molecular weight distribution are almost inevitable and limit the reproducibility of PSCs, hindering progress toward technology development and commercialization.[14–17] Small-molecule donors with their advantages of a well-defined molecular weight and easy purification suffer less from batch-to-batch variations and provide a possible solution to overcome this issue.[12,14–25] Recent progress in designing small-molecule donors, combined with control over phase separation and morphology, has pushed the PCEs of small-molecule organic solar cells (SM-OSCs) in which both donor and acceptor are well-defined small molecules to above of 15%, closing in on the existing efficiency gap with the best PSCs.[12,20,26]

OSCs generally include a photovoltaic active layer sandwiched between a transparent conductive oxide electrode, such as indium–tin oxide (ITO) or fluorine-doped tin oxide (FTO), and a metal electrode (Ag, Al, or Cu). To improve efficiency, often interface layers between the active layer and the electrodes are employed to enhance carrier extraction, especially for PSCs.[27–35] At the electron-collecting metal electrode, such layers are commonly referred to as cathode interlayers (CILs), a term that is unfortunately not correct because the anode is the negative terminal of the solar cell under operation. We will use the term electron transport layer (ETL). Several solution-processable organic molecules have been used as ETL to create a barrier-free contact between the metal electrode and the photovoltaic active layer, and improve device performance by decreasing the energy and recombination losses in charge extraction.[27,30,31,35–37] For example, Liao et al. developed a new ETL (S-3) by tailoring the 3,9-bis(2-methylene-(3-(1,1-dicyanomethylene)-indanone))-5,5,11,11-tetrakis(4-hexylphenyl)-dithieno[2,3-*d*:2′,3′-*d*′]-s-indaceno-[1,2-*b*:5,6-*b*′]-dithiophene) (ITIC) end-capping unit and thereby increased the PCE from 11.65% to 16.6%.[27] Recently, Yao et al. reported an ETL based on a hydrogen-bonding aliphatic-amine-functionalized perylenediimide (PDINN), which lowers the work function of the metal electrode and creates a good contact with the active layer. PSCs based on PDINN achieved a PCE of 17.23%, while the PDINN-free device shows a PCE of 13.39%.[38] Some other ETLs such as PDINO, poly(9,9-bis(3′-(*N*,*N*-dimethyl)-*N*-ethylammoinium-propyl-2,7-fluorene)-*alt*-2,7-(9,9-dioctylfluorene))dibromide (PFNBr), and poly[[2,7-bis(2-ethylhexyl)-1,2,3,6,7,8-hexahydro-1,3,6,8-tetraoxobenzo[lmn][3,8-phenanthroline-4,9-diyl]-2,5-thiophenediyl[9,9-bis[3-(dimethylamino)propyl]-9H-fluorene-2,7-diyl]-2,5-thiophenediyl] (PNDIT-F3N) are also widely used in highly efficient

Dr. H. Bin, Dr. J. Wang, Dr. J. Li, Dr. M. M. Wienk, Prof. R. A. J. Janssen
Molecular Materials and Nanosystems & Institute for Complex Molecular Systems
Eindhoven University of Technology
P.O. Box 513, Eindhoven 5600 MB, The Netherlands
E-mail: r.a.j.janssen@tue.nl
Prof. R. A. J. Janssen
Dutch Institute for Fundamental Energy Research
De Zaale 20, 5612 AJ, Eindhoven, The Netherlands
The ORCID identification number(s) for the author(s) of this article can be found under https://doi.org/10.1002/adma.202008429.

© 2021 The Authors. Advanced Materials published by Wiley-VCH GmbH. This is an open access article under the terms of the Creative Commons Attribution-NonCommercial License, which permits use, distribution and reproduction in any medium, provided the original work is properly cited and is not used for commercial purposes.

DOI: 10.1002/adma.202008429

15214095, 2021, 14, Downloaded from https://advanced.onlinelibrary.wiley.com/doi/10.1002/adma.202008429 by Junke Wang - Oxford University , Wiley Online Library on [28/03/2026]. See the Terms and Conditions (https://onlinelibrary.wiley.com/terms-and-conditions) on Wiley Online Library for rules of use; OA articles are governed by the applicable Creative Commons License

OSCs.[9,11,39–41] These examples illustrate that ETLs play an important role in PSCs and are seemingly indispensable to reach high PCEs.

However, despite various benefits, ETLs also introduce some disadvantages. First, because of their low conductivity, the functioning of ETLs is usually very sensitive to film thickness and, in general, ETLs only work well in ultrathin films of a few nanometers only. This is unfavorable for large-area roll-to-roll processing where such small thickness is difficult to control. Moreover, the polar solvents that are commonly used to deposit ETLs may affect the morphology of photoactive layers, while strong aggregation of some rigid π-conjugated ETL molecules can give poor device stability. Last but not least, the additional ETL complicates device fabrication and raises costs. Although considerable efforts have been devoted to developing ETL materials, not all issues have been overcome. To fully eliminate such challenges, efficient OSCs that operate without ETL can be an easy way out.[21,37,42,43]

Considering the low reproducibility caused by the batch-to-batch variations of polymers, and the necessity of ETLs in most PSCs, SM-OSCs are a promising platform for developing ETL-free OSCs. To this end, the design and synthesis of efficient organic small-molecule materials are essential. Thiophene-substituted benzodithiophene (BDTT) units have been widely applied in organic photovoltaic materials because of their excellent charge-transfer characteristics.[44] Introducing trialkylsilyl side chains on BDTT is a suitable strategy to deepen energy levels and improve crystallinity.[45–47] Herein, we present a novel small-molecule donor **H31** based on BDTT with trialkylsilyl side chains and use **H31** in a blend with the successful acceptor 2,2′-((2Z,2′Z)-((12,13-bis(2-ethylhexyl)-3,9-diundecyl-12,13-dihydro-[1,2,5]thiadiazolo[3,4-*e*]thieno[2″,3″:4′,5′]thieno[2′,3′:4,5]pyrrolo[3,2-g]thieno[2′,3′:4,5]thieno[3,2-*b*]indole-2,10-diyl)-bis(methanylylidene))bis(5,6-difluoro-3-oxo-2,3-dihydro-1H-indene-2,1-diylidene))dimalononitrile (Y6) to construct SM-OSCs. We demonstrate that **H31**:Y6 solar cells achieve PCEs of 13.6% without any ETL with superior long-term device stability. In contrast, if we utilize PDINO as ETL, the device shows a similar initial PCE of 13.2%, but the performance drops significantly with time. The results demonstrate that SM-OSCs not only have better reproducibility but also show advantages in low-cost processing and long-term stability, and thus form a promising candidate for the future commercial application of OSCs.

2. Results and Discussion

The molecular structures of **H31**, Y6 (BTP-4F), and PDINO are depicted in **Figure 1**a. **H31** was synthesized following the route depicted in Scheme S1 (Supporting Information) via two simple reactions in high yield. The first step is a Knoevenagel condensation and the second is a palladium-catalyzed Stille-coupling reaction. The synthetic procedures and characterization are described in the Supporting Information. **H31** shows good solubility in common organic solvents such as chloroform and chlorobenzene, and active layers were processed from solutions in chloroform. The UV–vis–NIR absorption spectra of **H31** thin films show a maximum at 558 nm with an onset at 660 nm,

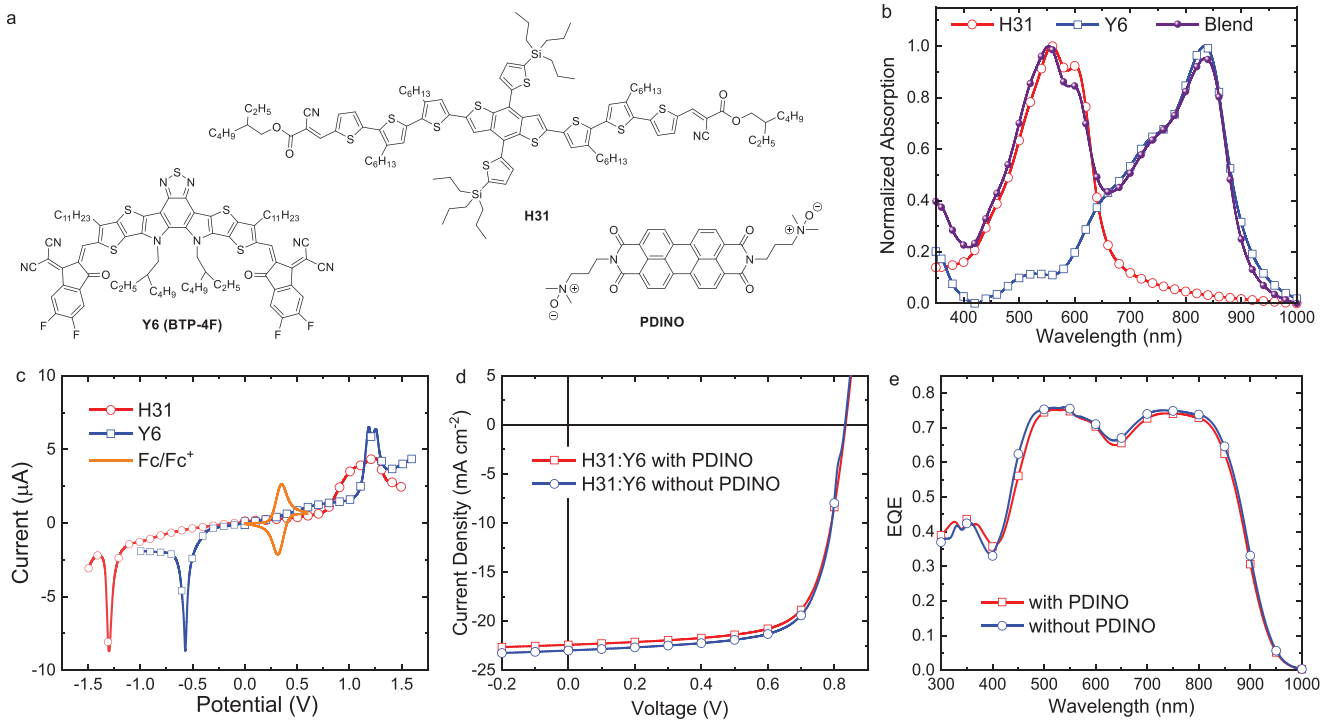

Figure 1. a) The chemical structures of **H31**, Y6, and PDINO. b) Optical absorption spectra of **H31**, Y6, and their blend in thin films. c) Square-wave voltammograms of **H31** and Y6 on a platinum wire in 0.1 mol L^{-1} Bu_4NPF_6 acetonitrile solutions at a scan rate of 20 mV s^{-1}. Potentials are versus Ag/AgCl. d) *J*–*V* characteristics of the PDINO-based and PDINO-free SM-OSCs, measured under simulated AM1.5G (100 mW cm^{-2}) illumination. e) EQE spectra of the corresponding devices.

© 2021 The Authors. Advanced Materials published by Wiley-VCH GmbH

15214095, 2021, 14, Downloaded from https://advanced.onlinelibrary.wiley.com/doi/10.1002/adma.202008429 by Junke Wang - Oxford University , Wiley Online Library on [28/03/2026]. See the Terms and Conditions (https://onlinelibrary.wiley.com/terms-and-conditions) on Wiley Online Library for rules of use; OA articles are governed by the applicable Creative Commons License

corresponding to an optical bandgap (E_g) of 1.88 eV (Figure 1b), while the absorbance of Y6 layers maximizes at 832 nm with an onset at 924 nm (E_g = 1.34 eV) (Figure 1b). The complementary absorption spectra of **H31** and Y6 make that blend films absorb over a wide spectral range, from 400 to 920 nm (Figure 1b), which is beneficial for obtaining a high short-circuit current density (J_{sc}).

The energy levels of **H31** and Y6 thin films deposited on a platinum wire were determined by square-wave voltammetry (SWV) (Figure 1c). The energies of the highest occupied molecular orbital (HOMO) and lowest unoccupied molecular orbital (LUMO) were determined from the onset potentials of the redox waves ($\varphi_{ox/red}$) versus Ag/AgCl as reference electrode. Absolute energies versus vacuum were obtained using ferrocene/ferrocenium as internal standard ($\varphi_{1/2}(Fc/Fc^+)$ = 0.37 eV vs Ag/AgCl) and using a value of −4.8 eV for Fc/Fc^+. The HOMO/LUMO energy levels are −5.21/−3.48 eV for **H31** and −5.54/−4.14 eV for Y6. The HOMO and LUMO offsets for **H31** and Y6 are 0.33 and 0.66 eV, sufficient for exciton dissociation.

The aggregation and crystallization of **H31** and Y6 were investigated by atomic force microscopy (AFM), 2D grazing-incidence wide-angle X-ray scattering (2D-GIWAXS), and differential scanning calorimetry (DSC). Neat **H31** films exhibit a surface topology with randomly distributed fibers and a root-mean-square surface roughness (R_q) larger than 5 nm, while pure Y6 films show a domain-like surface morphology with R_q ≈1.8 nm (Figure S1, Supporting Information). These results suggest a higher degree of aggregation for **H31** compared to Y6. In 2D-GIWAXS and the corresponding 1D line cuts, the **H31** film exhibits three distinct lamellar stacking peaks of at ≈0.35 $Å^{-1}$ (100), ≈0.68 $Å^{-1}$ (200), and ≈0.98 $Å^{-1}$ (300) in the out-of-plane (OOP) direction, together with an in-plane (IP) (010) peak at ≈1.69 $Å^{-1}$ corresponding to a π–π stacking distance (d_{010}) of 3.72 Å and a crystallite coherence length (CCL_{010}) of 22.6 Å (Figure S2, Supporting Information). This indicates that **H31** prefers an edge-on orientation. The splitting of the (200) and (300) peaks observed in the OOP direction is attributed to result from two different scattering pathways (dynamic effect) for X-rays in films of **H31**.[48] Thin films of Y6 show a predominant face-on orientation with a π–π stacking peak at 1.77 $Å^{-1}$ (d_{010} = 3.55 Å) in the OOP direction and CCL_{010} = 20.9 Å (Figure S2, Supporting Information), in accordance with previously reported results.[9,48] The 2D-GIWAXS results suggest a lower degree of molecular ordering and crystallinity for Y6 than for **H31** in thin films. DSC confirms the crystalline character of **H31** and Y6 because both exhibit a strong and narrow endothermic peak in the heating run at the melting point (Figure S3, Supporting Information). **H31** shows two exothermic peaks in the cooling run, indicating that it crystallizes from the melt, but Y6 does not show an exothermic peak upon cooling which may indicate decomposition in the melt or a hampered crystallization (Figure S3, Supporting Information).

A conventional device architecture consisting of ITO/poly(3,4-ethylenedioxythiophene)-poly(styrenesulfonate) (PEDOT:PSS)/active layer/PDINO (with or without)/Al was used to investigate the photovoltaic properties of **H31** and Y6 in SM-OSCs. The optimized conditions for depositing the active layer are a donor:acceptor weight ratio of 1:1 and a total blend concentration of 20 mg mL^{-1} in chloroform, spin coating at 1700 rpm for 60 s, followed by rapid thermal annealing at 140 °C for 1 min. SM-OSCs with and without PDINO interlayers have almost the same PCE as can be seen from the current density–voltage (J–V) characteristics (Figure 1d) and the photovoltaic parameters (PCE, open-circuit voltage (V_{oc}), J_{sc}, and fill factor (FF)) listed in **Table 1**. **H31**:Y6 solar cells with a PDINO interlayer provide a PCE of 13.2%, with V_{oc} = 0.83 V, J_{sc} = 22.4 mA cm^{-2}, and FF = 71%. The PDINO-free SM-OSC shows a similar PCE of 13.6%, with V_{oc} = 0.83 V, J_{sc} = 23.0 mA cm^{-2}, and FF = 71%. The external quantum efficiency (EQE) spectra of the PDINO-based and PDINO-free SM-OSCs were measured to determine J_{sc} independently. Both devices exhibit high incident photon-to-electron conversion efficiencies in the 300–900 nm wavelength range (Figure 1e) and the J_{sc} obtained by integration of the EQE spectra with the AM1.5G solar spectrum is in close correspondence with the value from J–V measurements (Table 1). The cells show a fairly small minimal photon energy loss (E_{loss}) of 0.51 eV, which is defined as the energy difference between E_g and qV_{oc}, where q is the elementary charge.

Table 1. Photovoltaic parameters of SM-OSCs measured with simulated AM1.5G (100 mW cm^{-2}) illumination.

Blend	J_{sc} [mA cm^{-2}]	V_{oc} [V]	FF	PCE[a] [%]	J_{sc}^{EQE} [mA cm^{-2}]	PCE^{EQE} [%]
H31:Y6[b]	22.4	0.83	0.71	13.2/12.9	22.5	13.3
H31:Y6[c]	23.0	0.83	0.71	13.6/13.2	23.0	13.6

[a]The two values represent the maximum PCE and the PCE averaged over ten different devices; [b]With PDINO; [c]Without PDINO.

Charge recombination was studied in PDINO-based and PDINO-free SM-OSCs by measuring the light intensity (P_{light}) dependence of J_{sc} and V_{oc}. The slope of J_{sc} versus P_{light} is close to unity in a double logarithmic plot for both devices (Figure S4a, Supporting Information), indicating little bimolecular recombination at short circuit. In a semilogarithmic plot, the slope of V_{oc} versus P_{light} is close to the thermal energy (kT/q, with k being the Boltzmann constant and T the absolute temperature) (Figure S4b, Supporting Information), suggesting that at open circuit charge recombination is primarily bimolecular or surface related rather than trap assisted. The excellent photovoltaic properties of the SM-OSCs are mainly due to a proper nanoscale phase separation and morphology and will discussed subsequently.

Similar high device performance was obtained using Ag instead of Al as top electrode (Figure S5 and Table S1, Supporting Information). Compared to Al, the Ag metal electrode gives a small increase in V_{oc} from 0.83 to 0.84 V, but reduces FF from 0.71 to 0.68 such that the PCE is slightly lower (12.6%). Remarkably also for Ag the use of PDINO as ETL did not affect the device performance. The **H31**:Y6 blend also shows very similar performance with PFNBr[49,50] as ETL (Figure S6, Supporting Information). The virtual identical initial PCEs and V_{oc}s obtained for **H31**:Y6 solar cells with Al, Ag, PDINO/Al, PDINO/Ag, and PFNBr/Al top contacts demonstrate that they are not strongly dependent on the presence or choice of the ETL.

Next to high efficiency, stability is important for future commercialization of OSCs. We studied the long-term stability (shelf life) of the two different device configurations in a

© 2021 The Authors. Advanced Materials published by Wiley-VCH GmbH

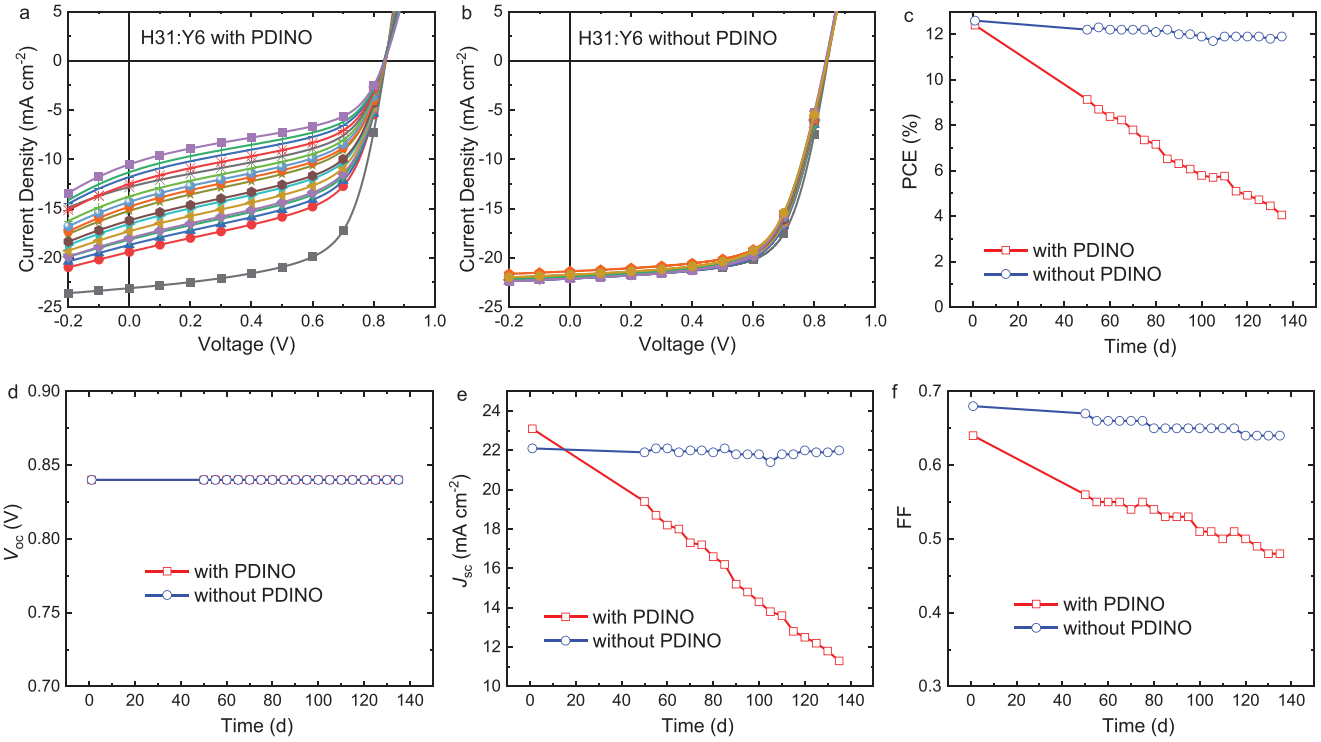

Figure 2. a,b) *J–V* curves of the PDINO-based (a) and ETL-free (b) SM-OSCs recorded over 140 days. c–f) The long-term stability of PCE, V_{oc}, J_{sc}, and FF of these two devices.

nitrogen atmosphere. The efficiency of the PDINO-based device degraded from 12.4% to only 4.1% after ≈140 days, presenting a 77% loss. In a sharp contrast, the efficiency of the PDINO-free device only shows a minor decrease in PCE from 12.6% to 11.9% and thus retains 94% of its initial performance. **Figure 2**a,b shows 18 *J–V* curves for each device configuration, taken over the course of 140 days. The performance of the PDINO-based device continuously degrades while the PDINO-free device shows near-overlapping *J–V* curves, indicating a much higher device stability. The photovoltaic parameters of the two devices versus time (Figure 2c–f) show that the decrease for the PDINO device is mainly due to severe drop of J_{sc} and FF. These changes may be related to changes in the active-layer morphology or in the nature of the interface with the electrodes.

To gain more insight into the molecular packing, orientation, and morphological stability, 2D-GIWAXS measurements for the blend films processed with and without PDINO on top were performed. Both blends exhibit the same π–π stacking peak at ≈1.64 Å^{-1} in the IP direction and at ≈1.74 Å^{-1} in the OOP direction (Figure S7a,b, Supporting Information). Comparison with the diffraction of the neat films suggests that these two reflections are dominated by **H31** and Y6, respectively. The peak positions and diffraction intensities do not change significantly with time for these blends (Figure S7c–h, Supporting Information), indicating that the bulk morphology of the two films is rather stable. Hence, the possibility that a change in the bulk morphology of the active layer causes the difference in device stability seems unlikely. This is corroborated by the constant V_{oc} of these two devices over 140 days (Figure 2d). In general, the V_{oc} is sensitive to morphological changes such as those created in postdeposition treatments in, e.g., thermal or solvent vapor annealing, and a constant V_{oc} can thus be taken as an indication that the morphology is stable.

To find the reason for widely different stability, the surface morphologies of blend films with/without PDINO were investigated by AFM in tapping mode. The AFM height and phase images of the blend films (**Figure 3**) indicate that initially the two blend films exhibit very similar surface morphologies. In both cases R_q is ≈2.40 nm, implying that PDINO does not change the surface morphology of the active layer. The excellent initial device performance shows that in cells with or without PDINO there is good physical and electrical contact between the active layer and the metal electrode. The efficient exciton dissociation and charge transport in the blends, inferred from the high FF and J_{sc}, show that near-optimal phase separation and 3D morphology are present initially. However, the situation changes after aging. After 30 days, PDINO-free blend films still exhibit smooth and uniform surfaces comparable to initial films, and even after 60 days there are only minor differences. In contrast, blend films with PDINO at the top surface show band-like textures in the height and phase images after 30 days, indicating that the surface morphology has changed. By extending the aging to 60 days even spikes and streaks are observed in the AFM, demonstrating that the surface deteriorates. This surface modification is the likely reason for the decreased J_{sc}, FF, and PCE of the PDINO-based devices. In AFM measurements on neat PDINO films (Figure S8, Supporting Information), similar band-like textures can be observed. We assume that due to its rigid core PDINO aggregates with time, leading to an unstable surface morphology that degrades device performance. Apparently, this aggregation not only occurs for **H31**:Y6 films covered

© 2021 The Authors. Advanced Materials published by Wiley-VCH GmbH

15214095, 2021, 14, Downloaded from https://advanced.onlinelibrary.wiley.com/doi/10.1002/adma.202008429 by Junke Wang - Oxford University , Wiley Online Library on [28/03/2026]. See the Terms and Conditions (https://onlinelibrary.wiley.com/terms-and-conditions) on Wiley Online Library for rules of use; OA articles are governed by the applicable Creative Commons License

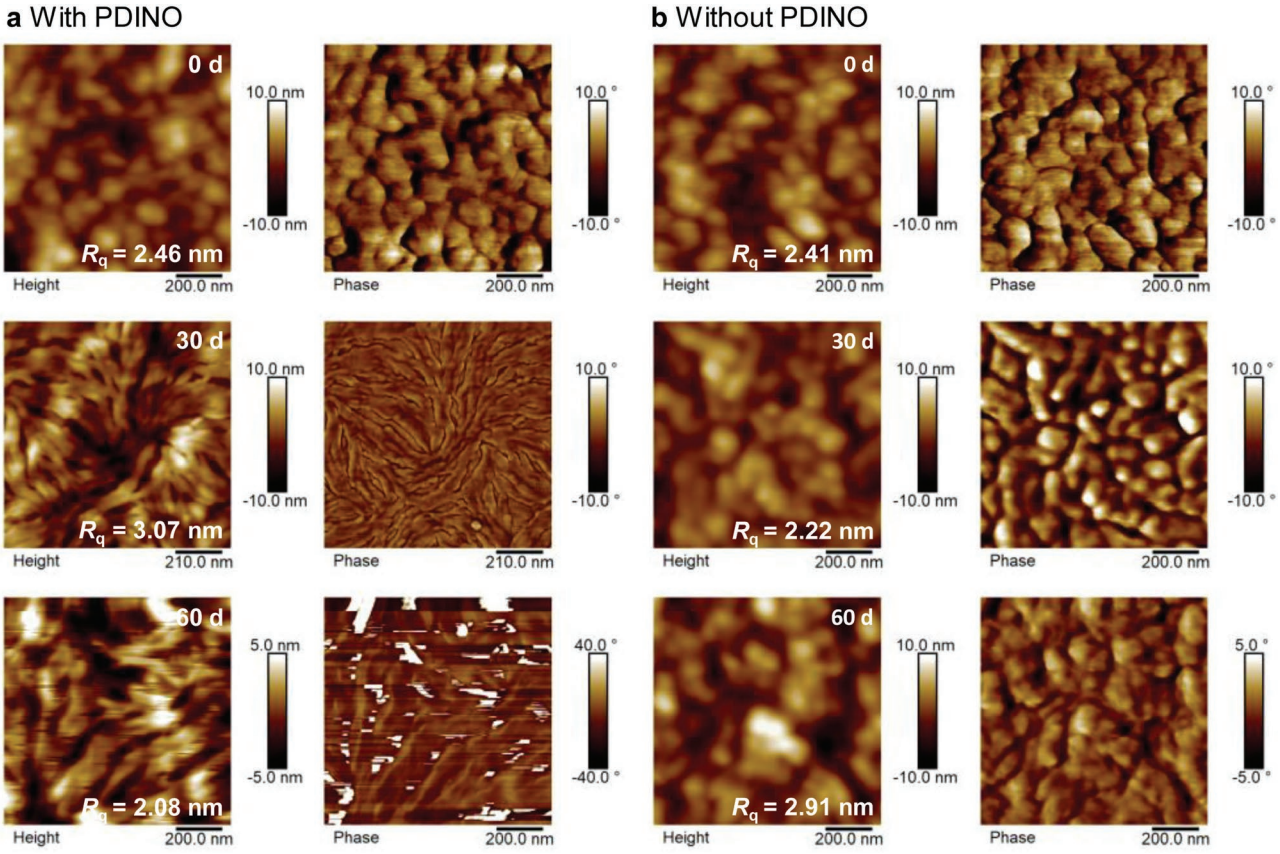

Figure 3. a,b) AFM height and phase images of fresh (0 days) and aged (30 and 60 days) **H31**:Y6 blend films with (a) or without (b) PDINO on the top surface.

with PDINO exposed to a N_2 atmosphere, but also when these films are covered with an Al electrode.

X-ray photoelectron spectroscopy (XPS) was used to study the distribution of **H31**, Y6, and PDINO at the top surface of the blend films to further examine the degradation. High-resolution XPS scans of neat **H31** and Y6 films without/with PDINO and the resulting atomic concentrations (Figure S9 and Table S2, Supporting Information) reveal that N and O concentrations increase significantly when covering neat films with PDINO as expected from the molecular structures, while the concentration of tracer elements, Si for the **H31** donor and F of the Y6 acceptor, decreases accordingly. The surface changes and degradation can be seen in more detail from the individual high-resolution XPS scans of N 1s, O 1s, F 1s, and Si 2p for fresh and aged blend films processed without and with PDINO (**Figure 4**; Table S2, Supporting Information).[51–53] First, for fresh and aged PDINO-free blend films, the XPS spectra and the atomic concentrations show negligible changes over time, confirming the stability of the surface composition. In contrast, XPS spectra for fresh and aged blend films with PDINO on top exhibit clear differences, especially for signals associated with pyrrolic-N and N—O species (Figure 4e,f). This demonstrates that the top surface is not stable when using PDINO. Second, for the PDINO-covered blend films, the intensity of the pyrrolic-N and C=O signals increases with time, with a concomitant decrease of N—O signals. This implies that PDINO may partially decompose. Third, the atomic concentrations at the surface for N, O, F, and Si in PDINO-free and PDINO-based blends do not change significantly with aging (Table S2, Supporting Information). This indicates that **H31**, Y6, and PDINO do not migrate in the vertical direction. This implies that all changes may be due to aggregation or chemical transformations at the top surface. In conclusion, XPS reveals a superior stability of the surface chemistry of PDINO-free blend films and comparatively poor stability of PDINO-covered blend films, in good correlation with results from AFM and device stability.

The chemical stability of PDINO was verified in methanol solution. PDINO easily dissolves in methanol and provides a clear light-red solution. When the solution is stored in a N_2-filled glovebox for 3 weeks, the color fades, the solution becomes cloudy, and some insoluble particles form (Figure S10, Supporting Information). The matrix-assisted laser-desorption/ionization time-of-flight (MALDI-TOF) mass spectrum of PDINO from a fresh solution shows the expected peak at m/z = 591.4 amu (Figure S11, Supporting Information), but an aged sample gave a complex mass spectrum showing several peaks with m/z values less than 591.4 amu. This demonstrates that PDINO decomposes in methanol. The poor chemical stability of PDINO could contribute to the unstable top surface chemistry.

Future commercialization of OSCs requires high efficiency, excellent stability, insensitivity to air, and compatibility with large-area roll-to-roll processing. To this end, we explored the photovoltaic performance of PDINO-free SM-OSCs processed under ambient conditions and at larger areas. When the active

© 2021 The Authors. Advanced Materials published by Wiley-VCH GmbH

15214095, 2021, 14, Downloaded from https://advanced.onlinelibrary.wiley.com/doi/10.1002/adma.202008429 by Junke Wang - Oxford University , Wiley Online Library on [28/03/2026]. See the Terms and Conditions (https://onlinelibrary.wiley.com/terms-and-conditions) on Wiley Online Library for rules of use; OA articles are governed by the applicable Creative Commons License

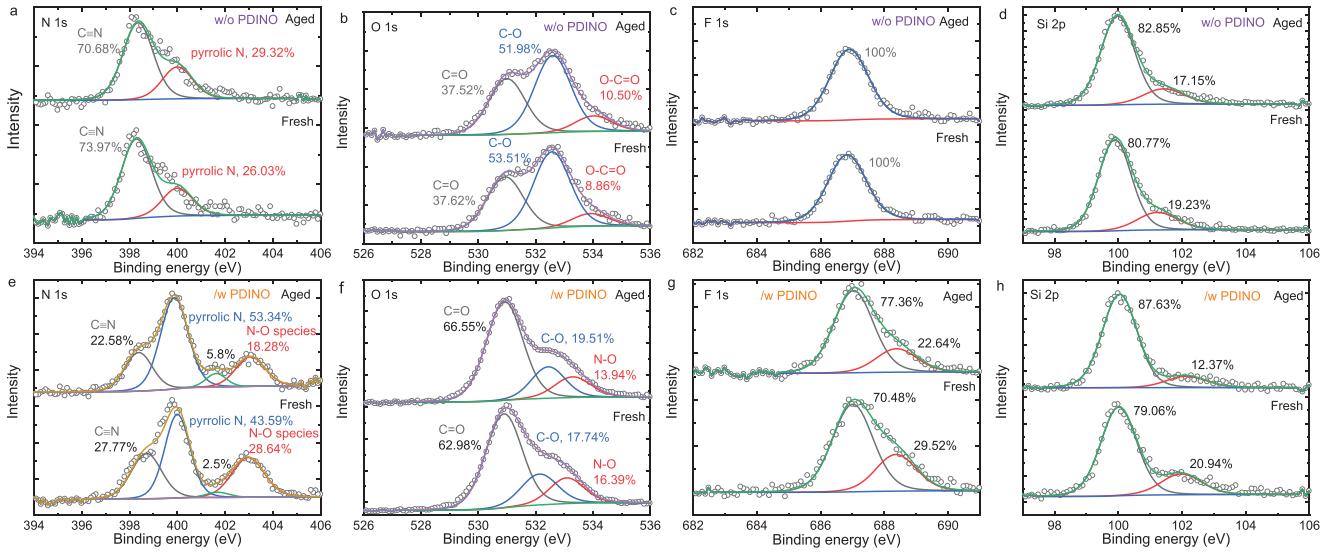

Figure 4. a–h) High-resolution XPS scans of the atomic core levels for fresh and aged blend films with and without PDINO on top: a,e) N 1s; b,f) O 1s; c,g) F 1s; d,h) Si 2p.

layer and PDINO are spin-coated under ambient conditions (21 °C, 24% relative humidity), PDINO-free cells provide a PCE of 10.8%, with V_{oc} = 0.83 V, J_{sc} = 21.8 mA cm^{-2}, and FF = 60% (Figure S12, Supporting Information). This is much higher than for the PDINO-based device, which reaches a PCE of 7.3%. Likewise, larger area (1 cm^2) PDINO-free SM-OSCs show a better PCE of 8.8%, compared to PDINO-based cells with a PCE of 6.1%. Although the air sensitivity and large-area processing still leave considerable room for improvement, the electrode interlayer-free devices consistently outperform the PDINO-based cells. We further studied the universality of the ETL-free SM-OSCs with other active layers, including H11:IDIC-4F and H22:Y6 (structures shown in Figure S13 in the Supporting Information). By comparing device performance and stability of the SM-OSCs with/without PDINO within these two different active layers (Figure S14 and Table S3, Supporting Information), we found the ETL-free devices show comparable initial device performance and better device stability, indicating that well performing the ETL-free SM-OSCs is not restricted to the **H31**:Y6 combination studied here in detail. We also investigated the device performance of PSCs based on blends of two polymers, J71-Cl and J101[54] (structures shown in Figure S15 in the Supporting Information), with 9-bis(2-methylene-((3-(1,1-dicyanomethylene)-6,7-difluoro)-indanone))-5,5,11,11-tetrakis(4-hexylphenyl)-dithieno[2,3-*d*:2′,3′-*d*′]-s-indaceno[1,2-*b*:5,6-*b*′]dithiophene (IT-4F) as NFA with and without PDINO and found that both PSCs show lower PCEs without PDINO (Figure S16 and Table S4, Supporting Information). This demonstrates that PDINO enhances the PCE in these PSCs. A similar result was reported recently for a blend of poly[(2,6-(4,8-bis(5-(2-ethylhexyl-3-fluoro)thiophen-2-yl)-benzo[1,2-*b*:4,5-*b*′]dithiophene))-*alt*-(5,5-(1′,3′-di-2-thienyl-5′,7′-bis(2-ethylhexyl)benzo[1′,2′-*c*:4′,5′-*c*′] dithiophene-4,8-dione)] (PM6) and Y6.[38] This shows that omitting the ETL affects the initial performance in these PSCs negatively. So far it is difficult to predict in which case the ETL can be omitted. There seems to be a difference between PSCs and SM-OSCs. Remarkably, it does not depend on the acceptor because for Y6 no ETL is required when combined with **H31** in SM-OCS but it is necessary with PM6 in a PSC.[38]

It is of interest to understand what is the underlying mechanism and why in some cases the ETL can be omitted. For **H31**:Y6 cells we observe no significant difference between Al and PDINO/Al top contacts in initial device performance or light intensity dependences. The two contacts behave very similar, and without a difference it is not easy to investigate the mechanism. Also in other reports of efficient SM-OSCs without ETL, the reasons for the identical performance remained elusive.[21,43]

3. Conclusion

A new small-molecule donor **H31** based on a BDTT core unit with trialkylsilyl side chains exhibits a deep HOMO energy level and a complementary absorption spectrum with the non-fullerene acceptor Y6. Blending **H31** and Y6 gives efficient SM-OSCs (with/without ETLs) with PCEs over 13%, ascribed to a small minimal photon energy loss and an appropriate phase-separated nanomorphology, in which the 3D structure affords efficient charge generation and collection pathways and suppresses recombination. ETL-free SM-OSCs deliver a superior shelf-life stability compared to devices that use PDINO as ETL. Without PDINO, time-stable bulk and surface morphologies are obtained, while devices with PDINO as ETL deteriorate quickly. 2D-GIWAXS, AFM, and XPS measurements reveal that the poor stability is caused by the aggregation and decomposition of PDINO, leading to an unstable top surface topology and chemistry, resulting in a fast degradation of J_{sc} and FF. ETL-free devices show potential for larger-area devices and reduced air sensitivity. The results demonstrate that small-molecule donor–acceptor blends provide interesting perspectives for achieving efficient, reproducible, and stable device architectures by omitting electrode interlayers.

© 2021 The Authors. Advanced Materials published by Wiley-VCH GmbH

15214095, 2021, 14, Downloaded from https://advanced.onlinelibrary.wiley.com/doi/10.1002/adma.202008429 by Junke Wang - Oxford University , Wiley Online Library on [28/03/2026]. See the Terms and Conditions (https://onlinelibrary.wiley.com/terms-and-conditions) on Wiley Online Library for rules of use; OA articles are governed by the applicable Creative Commons License

Supporting Information

Supporting Information is available from the Wiley Online Library or from the author.

Acknowledgements

The research received funding from the Netherlands Organisation for Scientific Research via an NWO Spinoza grant. The authors further acknowledge funding from the Ministry of Education, Culture and Science (Gravity program 024.001.035).

Conflict of Interest

The authors declare no conflict of interest.

Data Availability Statement

Research data are not shared.

Keywords

degradation, electrode interlayers, organic semiconductors, organic solar cells, stability

Received: December 14, 2020
Revised: January 27, 2021
Published online: March 3, 2021

[1] R. Ma, T. Liu, Z. Luo, Q. Guo, Y. Xiao, Y. Chen, X. Li, S. Luo, X. Lu, M. Zhang, Y. Li, H. Yan, *Sci. China: Chem.* **2020**, *63*, 325.
[2] Q. Liu, Y. Jiang, K. Jin, J. Qin, J. Xu, W. Li, J. Xiong, J. Liu, Z. Xiao, K. Sun, S. Yang, X. Zhang, L. Ding, *Sci. Bull.* **2020**, *65*, 272.
[3] L. Liu, Y. Kan, K. Gao, J. Wang, M. Zhao, H. Chen, C. Zhao, T. Jiu, A. K. Y. Jen, Y. Li, *Adv. Mater.* **2020**, *32*, 1907604.
[4] L. Meng, Y. Zhang, X. Wan, C. Li, X. Zhang, Y. Wang, X. Ke, Z. Xiao, L. Ding, R. Xia, H. L. Yip, Y. Cao, Y. Chen, *Science* **2018**, *361*, 1094.
[5] Y. Lin, B. Adilbekova, Y. Firdaus, E. Yengel, H. Faber, M. Sajjad, X. Zheng, E. Yarali, A. Seitkhan, O. M. Bakr, A. El-Labban, U. Schwingenschlögl, V. Tung, I. McCulloch, F. Laquai, T. D. Anthopoulos, *Adv. Mater.* **2019**, *31*, 1902965.
[6] Y. Cui, H. Yao, J. Zhang, K. Xian, T. Zhang, L. Hong, Y. Wang, Y. Xu, K. Ma, C. An, C. He, Z. Wei, F. Gao, J. Hou, *Adv. Mater.* **2020**, *32*, 1908205.
[7] L. Zhan, S. Li, T. K. Lau, Y. Cui, X. Lu, M. Shi, C. Z. Li, H. Li, J. Hou, H. Chen, *Energy Environ. Sci.* **2020**, *13*, 635.
[8] C. Zhu, J. Yuan, F. Cai, L. Meng, H. Zhang, H. Chen, J. Li, B. Qiu, H. Peng, S. Chen, Y. Hu, C. Yang, F. Gao, Y. Zou, Y. Li, *Energy Environ. Sci.* **2020**, *13*, 2459.
[9] J. Yuan, Y. Zhang, L. Zhou, G. Zhang, H. L. Yip, T. K. Lau, X. Lu, C. Zhu, H. Peng, P. A. Johnson, M. Leclerc, Y. Cao, J. Ulanski, Y. Li, Y. Zou, *Joule* **2019**, *3*, 1140.
[10] H. Lai, Q. Zhao, H. Lai, Q. Zhao, Z. Chen, H. Chen, P. Chao, Y. Zhu, Y. Lang, *Joule* **2020**, *4*, 688.
[11] Z. Luo, R. Ma, Z. Luo, R. Ma, T. Liu, J. Yu, Y. Xiao, R. Sun, G. Xie, *Joule* **2020**, *4*, 1236.
[12] L. Nian, Y. Kan, F. Liu, G. Zhou, A. K. Jen, L. Nian, Y. Kan, K. Gao, M. Zhang, N. Li, G. Zhou, S. B. Jo, X. Shi, F. Lin, Q. Rong, F. Liu, G. Zhou, A. K. Y. Jen, *Joule* **2020**, *4*, 2223.
[13] J. Wu, G. Li, J. Fang, X. Guo, L. Zhu, B. Guo, Y. Wang, G. Zhang, L. Arunagiri, F. Liu, H. Yan, M. Zhang, Y. Li, *Nat. Commun.* **2020**, *11*, 4612.
[14] H. Bin, Y. Yang, Z. G. Zhang, L. Ye, M. Ghasemi, S. Chen, Y. Zhang, C. Zhang, C. Sun, L. Xue, C. Yang, H. Ade, Y. Li, *J. Am. Chem. Soc.* **2017**, *139*, 5085.
[15] J. Guo, H. Bin, W. Wang, B. Chen, J. Guo, R. Sun, Z. G. Zhang, X. Jiao, Y. Li, J. Min, *J. Mater. Chem. A* **2018**, *6*, 15675.
[16] H. Bin, I. Angunawela, B. Qiu, F. J. M. Colberts, M. Li, M. J. Dyson, M. M. Wienk, H. Ade, Y. Li, R. A. J. Janssen, *Adv. Energy Mater.* **2020**, *10*, 2001589.
[17] H. Bin, J. Yao, Y. Yang, I. Angunawela, C. Sun, L. Gao, L. Ye, B. Qiu, L. Xue, C. Zhu, C. Yang, Z. G. Zhang, H. Ade, Y. Li, *Adv. Mater.* **2018**, *30*, 1706361.
[18] H. Li, Q. Wu, R. Zhou, Y. Shi, C. Yang, Y. Zhang, J. Zhang, W. Zou, D. Deng, K. Lu, Z. Wei, *Adv. Energy Mater.* **2019**, *9*, 1803175.
[19] Y. Wang, Y. Wang, B. Kan, X. Ke, X. Wan, C. Li, Y. Chen, *Adv. Energy Mater.* **2018**, *8*, 1802021.
[20] J. Qin, C. An, J. Zhang, K. Ma, Y. Yang, T. Zhang, S. Li, K. Xian, Y. Cui, Y. Tang, W. Mai, H. Yao, S. Zhang, B. Xu, C. He, J. Hui, *Sci. China Mater.* **2020**, *63*, 1142.
[21] R. Zhou, Z. Jiang, C. Yang, J. Yu, J. Feng, M. A. Adil, D. Deng, W. Zou, J. Zhang, K. Lu, W. Ma, F. Gao, Z. Wei, *Nat. Commun.* **2019**, *10*, 5393.
[22] K. Gao, S. B. Jo, X. Shi, L. Nian, M. Zhang, Y. Kan, F. Lin, B. Kan, B. Xu, Q. Rong, L. Shui, F. Liu, X. Peng, G. Zhou, Y. Cao, A. K. Y. Jen, *Adv. Mater.* **2019**, *31*, 1807842.
[23] H. Chen, D. Hu, Q. Yang, J. Gao, J. Fu, K. Yang, H. He, S. Chen, Z. Kan, T. Duan, C. Yang, J. Ouyang, Z. Xiao, K. Sun, S. Lu, *Joule* **2019**, *3*, 3034.
[24] Y. Huo, H. L. Zhang, X. Zhan, *ACS Energy Lett.* **2019**, *4*, 1241.
[25] X. Dong, K. Yang, H. Tang, D. Hu, S. Chen, J. Zhang, Z. Kan, T. Duan, C. Hu, X. Dai, Z. Xiao, K. Sun, S. Lu, *Sol. RRL* **2019**, *4*, 1900326.
[26] D. Hu, Q. Yang, H. Chen, F. Wobben, V. M. Le Corre, R. Singh, T. Liu, R. Ma, H. Tang, L. J. A. Koster, T. Duan, H. Yan, Z. Kan, Z. Xiao, S. Lu, *Energy Environ. Sci.* **2020**, *13*, 2134.
[27] Q. Liao, Q. Kang, Y. Yang, C. An, B. Xu, J. Hou, *Adv. Mater.* **2020**, *32*, 1906557.
[28] Y. Liu, V. V. Duzhko, Z. A. Page, T. Emrick, T. P. Russell, *Acc. Chem. Res.* **2016**, *49*, 2478.
[29] S. Liu, K. Zhang, J. Lu, J. Zhang, H. L. Yip, F. Huang, Y. Cao, *J. Am. Chem. Soc.* **2013**, *135*, 15326.
[30] Z. Li, D. Yang, X. Zhao, Z. Li, T. Zhang, F. Wu, X. Yang, *RSC Adv.* **2016**, *6*, 101645.
[31] Z. Ding, Z. Miao, Z. Xie, J. Liu, *J. Mater. Chem. A* **2016**, *4*, 2413.
[32] L. Nian, W. Zhang, N. Zhu, L. Liu, Z. Xie, H. Wu, F. Würthner, Y. Ma, *J. Am. Chem. Soc.* **2015**, *137*, 6995.
[33] B. Xiao, H. Wu, Y. Cao, *Mater. Today* **2015**, *18*, 385.
[34] K. Zhao, L. Ye, W. Zhao, S. Zhang, H. Yao, B. Xu, M. Sun, J. Hou, *J. Mater. Chem. C* **2015**, *3*, 9565.
[35] Q. Kang, L. Ye, B. Xu, C. An, S. J. Stuard, S. Zhang, H. Yao, H. Ade, J. Hou, *Joule* **2019**, *3*, 227.
[36] J. Han, Y. Chen, W. Chen, C. Yu, X. Song, F. Li, Y. Wang, *ACS Appl. Mater. Interfaces* **2016**, *8*, 32823.
[37] X. Chen, B. Zhu, B. Kan, K. Gao, X. Peng, Y. Cao, *J. Mater. Chem. C* **2019**, *7*, 7947.
[38] J. Yao, B. Qiu, Z. G. Zhang, L. Xue, R. Wang, C. Zhang, S. Chen, Q. Zhou, C. Sun, C. Yang, M. Xiao, L. Meng, Y. Li, *Nat. Commun.* **2020**, *11*, 2726.
[39] Z. G. Zhang, B. Qi, Z. Jin, D. Chi, Z. Qi, Y. Li, J. Wang, *Energy Environ. Sci.* **2014**, *7*, 1966.
[40] H. Yao, Y. Cui, D. Qian, C. S. Ponseca, A. Honarfar, Y. Xu, J. Xin, Z. Chen, L. Hong, B. Gao, R. Yu, Y. Zu, W. Ma, P. Chabera, T. Pullerits, A. Yartsev, F. Gao, J. Hou, *J. Am. Chem. Soc.* **2019**, *141*, 7743.
[41] Z. Wu, C. Sun, S. Dong, X. F. Jiang, S. Wu, H. Wu, H. L. Yip, F. Huang, Y. Cao, *J. Am. Chem. Soc.* **2016**, *138*, 2004.

© 2021 The Authors. Advanced Materials published by Wiley-VCH GmbH

15214095, 2021, 14, Downloaded from https://advanced.onlinelibrary.wiley.com/doi/10.1002/adma.202008429 by Junke Wang - Oxford University , Wiley Online Library on [28/03/2026]. See the Terms and Conditions (https://onlinelibrary.wiley.com/terms-and-conditions) on Wiley Online Library for rules of use; OA articles are governed by the applicable Creative Commons License

[42] H. Zhou, Y. Zhang, J. Seifter, S. D. Collins, C. Luo, G. C. Bazan, T. Q. Nguyen, A. J. Heeger, *Adv. Mater.* **2013**, *25*, 1646.
[43] H. Wu, Q. Yue, Z. Zhou, S. Chen, D. Zhang, S. Xu, H. Zhou, C. Yang, H. Fan, X. Zhu, *J. Mater. Chem. A* **2019**, *7*, 15944.
[44] H. Yao, L. Ye, H. Zhang, S. Li, S. Zhang, J. Hou, *Chem. Rev.* **2016**, *116*, 7397.
[45] H. Bin, L. Gao, Z. G. Zhang, Y. Yang, Y. Zhang, C. Zhang, S. Chen, L. Xue, C. Yang, M. Xiao, Y. Li, *Nat. Commun.* **2016**, *7*, 13651.
[46] H. Bin, Y. Yang, Z. Peng, L. Ye, J. Yao, L. Zhong, C. Sun, L. Gao, H. Huang, X. Li, B. Qiu, L. Xue, Z. G. Zhang, H. Ade, Y. Li, *Adv. Energy Mater.* **2018**, *8*, 1702324.
[47] T. Yan, H. Bin, C. Sun, Z. G. Zhang, Y. Li, *Org. Electron.* **2018**, *57*, 255.
[48] R. Resel, M. Bainschab, A. Pichler, T. Dingemans, C. Simbrunner, J. Stangl, I. Salzmann, *J. Synchrotron Radiat.* **2016**, *23*, 729.
[49] F. Huang, H. Wu, D. Wang, W. Yang, Y. Cao, *Chem. Mater.* **2004**, *16*, 708.
[50] H. Wu, F. Huang, Y. Mo, W. Yang, D. Wang, J. Peng, Y. Cao, *Adv. Mater.* **2004**, *16*, 1826.
[51] W. Zhu, A. P. Spencer, S. Mukherjee, J. M. Alzola, V. K. Sangwan, S. H. Amsterdam, S. M. Swick, L. O. Jones, M. C. Heiber, A. A. Herzing, G. Li, C. L. Stern, D. M. DeLongchamp, K. L. Kohlstedt, M. C. Hersam, G. C. Schatz, M. R. Wasielewski, L. X. Chen, A. Facchetti, T. J. Marks, *J. Am. Chem. Soc.* **2020**, *142*, 14532.
[52] J. Wang, K. Datta, C. H. L. Weijtens, M. M. Wienk, R. A. J. Janssen, *Adv. Funct. Mater.* **2019**, *29*, 1905883.
[53] H. Alhummiany, S. Rafique, K. Sulaiman, *J. Phys. Chem. C* **2017**, *121*, 7649.
[54] H. Bin, I. Angunawela, R. Ma, A. Nallapaneni, C. Zhu, P. J. Leenaers, B. W. H. Saes, M. M. Wienk, H. Yan, H. Ade, R. A. J. Janssen, *J. Mater. Chem. C* **2020**, *8*, 15426.

© 2021 The Authors. Advanced Materials published by Wiley-VCH GmbH

15214095, 2021, 14, Downloaded from https://advanced.onlinelibrary.wiley.com/doi/10.1002/adma.202008429 by Junke Wang - Oxford University , Wiley Online Library on [28/03/2026]. See the Terms and Conditions (https://onlinelibrary.wiley.com/terms-and-conditions) on Wiley Online Library for rules of use; OA articles are governed by the applicable Creative Commons License